RADIATIVE TRANSFER IN THE CO-MOVING FRAME

A. PERAIAH

Indian Institute of Astrophysics, Bangalore, India

(Received 11 November, 1980)

Abstract. Solution of line-transfer equation in the co-moving frame, obtained on the basis of discrete space theory, has been employed to calculate the lines emerging from a rapidly expanding stellar atmosphere. The solution is found to be highly stable for large velocities of expansion with both positive and negative velocity gradients. We have presented profiles of spectral lines that are translated along the line of sight of the observer at infinity. We have treated a Non-LTE two-level atom in a medium scattering isotropically with line and continuum emission. P Cygni-type profiles noticed in a purely scattering medium.

1. Introduction

The atmospheres of Wolf-Rayet stars, P Cygni-type stars, quasars, novae and other objects are well known to be expanding outwards. The computation of spectral lines emerging from such media is rather a difficult task. In recent times, there have been several attempts at finding a solution to these problems (see, e.g., Kunasz and Hummer, 1974; Peraiah, 1978; and others). These calculations have been done in the rest frame of the star and there are several practical difficulties with this approach. For example, when the velocity of the gas becomes larger than, say, 2 or 3 mean thermal units (mtu), the frequency angle mesh becomes quite large and this requires large storage and time on the computer. This becomes unmanageable, particularly when the line-centre optical depths are of the order 10^4 or 10^5.

Consequently, one is forced to consider the problem of line formation in a rapidly expanding media in the co-moving frame of the expanding gas. In this frame, the observer need not account for the Doppler shifts which directly enters into the absorption coefficient (in the rest frame) and the calculation of photon redistribution in the line become easy. However, one has to translate the lines formed in this frame on to the rest frame of the star – if one wishes to calculate the spherically-symmetric solution of the radiative transfer equation in the expanding medium or on to the line of sight of the observer at infinity for direct comparison with observations. Simmonneau (1973) and Mihalas *et al.* (1975) have found a solution of line transfer in the co-moving frame. However, these techniques seem to be complicated and require more computing time than warranted and it appears that one has to be careful about the velocity laws.

A direct numerical solution of line radiative transfer equation in a co-moving frame has been developed in the framework of discrete space theory (Peraiah, 1980a, 1980b; henceforth referred to as Papers I and II, respectively). This is

Astrophysics and Space Science **77** (1981) 243–255. 0004–640X/81/0771–0243$01.95.

numerically stable and can deal with arbitrary velocity laws in the expanding media. In this paper, we describe the lines formed in a media which are expanding and decelerating with gas velocities as large as 100 mean thermal units.

2. Brief Description of the Solution of Radiative Transfer in the Co-moving Frame

Details of the solution in a co-moving frame are given in Papers I and II. We shall give a brief sketch of the method of obtaining the solution. The equation of line transfer in the co-moving frame is given by

$$\mu \frac{\partial I(x,\mu,r)}{\partial r} + \frac{1-\mu^2}{r} \frac{\partial I(x,\mu,r)}{\partial \mu} = k_l[\beta + \phi(x)] \times$$
$$\times [S(x,r) - I(x,\mu,r)] + \left\{(1-\mu^2)\frac{V(r)}{r} + \mu^2 \frac{\mathrm{d}V(r)}{\mathrm{d}r}\right\} \frac{\partial I(x,\mu,r)}{\partial x} \qquad (1)$$

and

$$-\mu \frac{\partial I(x,-\mu,r)}{\partial r} - \frac{1-\mu^2}{r} \frac{\partial I(x,-\mu,r)}{\partial \mu} = k_l[\beta + \phi(x)] \times$$
$$\times [S(x,r) - I(x,-\mu,r)] + \left\{(1-\mu^2)\frac{V(r)}{r} + \mu^2 \frac{\mathrm{d}V(r)}{\mathrm{d}r}\right\} \frac{\partial I(x,-\mu,r)}{\partial x} , \qquad (2)$$

where $I(x,\mu,r)$ is the specific intensity making an angle $\cos^{-1}\mu$ with the radius vector at the radial point r for the frequency $x(=(\nu-\nu_0)/\Delta_S$, Δ_S being some standard frequency interval); and $V(r)$ is the velocity of the gas at radius r in mean thermal velocity units. The function $\phi(x)$ stands for the line profile given by

$$\phi(x) = \frac{1}{\delta\sqrt{\pi}} \, \mathrm{e}^{-x^2/\delta^2} , \qquad (3)$$

where δ is the ratio $\Delta_S(r)/\Delta_S$ and δ is always kept equal to unity. The profile is normalized so that

$$\int_{-\infty}^{+\infty} \phi(x)\,\mathrm{d}x = 1 \ ; \qquad (4)$$

$S(x,\mu,r)$ being the source function given by

$$S(x,r) = \frac{\phi(x)}{\beta+\phi(x)} \, S_L(r) + \frac{\beta}{\beta+\phi(x)} \, S_C(r) \ ; \qquad (5)$$

with $S_L(r)$ and $S_C(r)$ denoting the lines and continuum-source functions; and β is the quantity k_C/k_L where k_C and k_L are the continuum and line absorption coefficients per unit frequency intervals. We can set $S_C(r) = B(r)$, where the

Planck function and the line source function is calculated by

$$S_L(r) = \tfrac{1}{2}(1-\epsilon)\int_{-\infty}^{+\infty}\phi(x)\,dx\int_{-1}^{+1} I(x,\mu,r)\,d\mu + \epsilon B(r)\ , \tag{6}$$

where ϵ is the photon destruction probability by collisional de-excitation. We have solved Equations (1) and (2) by discretization as described in Paper I. The co-moving terms

$$\left\{(1-\mu^2)\frac{V(r)}{r} + \mu^2\frac{dV(r)}{dr}\right\}\frac{\partial I(x,\pm\mu,r)}{\partial x}$$

are discretized and put in the term $\mathbf{M}_1\mathbf{du}^{\pm}$, where

$$\mathbf{M}_1 = [\mathbf{M}^1\,\Delta V_{n+(1/2)} + \mathbf{M}^2\rho_c V_{n+(1/2)}]\ , \tag{8}$$

$$\mathbf{M}^1 = \begin{bmatrix} \mathbf{M}^1_m & & & \\ & \mathbf{M}^1_m & & \\ & & \ddots & \\ & & & \mathbf{M}^1_m \end{bmatrix}, \tag{9}$$

$$\mathbf{M}^2 = \begin{bmatrix} \mathbf{M}^2_m & & & \\ & \mathbf{M}^2_m & & \\ & & \ddots & \\ & & & \mathbf{M}^2_m \end{bmatrix}, \tag{10}$$

$$\left.\begin{aligned} M^1_m &= [\mu_j^2\delta_{jl}] \\ M^2_m &= [(1-\mu_j^2)\delta_{jl}] \end{aligned}\right\},\quad j,l = 1,2,\ldots,J\ ; \tag{11}$$

where ρ_c is the curvature factor given by $\rho_c = \Delta r/r_{n+(1/2)}$, $\Delta V_{n+(1/2)}$ is the radial velocity difference $V_{n+1} - V_n$ where V_{n+1}, and V_n represent the velocities at r_{n+1} and r_n, respectively, while $V_{n+(1/2)}$ is the average velocity over the shell bounded by the radii r_{n+1} and r_n. The quantity $\mathbf{d}$ is the discretized form of the derivative $\partial I(x,\mu,r)/\partial x$. This has been obtained by considering the condition of flux conservation in a purely scattering medium and is given (see Papers I and II) by

$$\mathbf{d} = \begin{bmatrix} -d_1 & d_1 & & & \\ -d_2 & 0 & d_2 & & \\ & -d_3 & 0 & d_3 & \\ & & & & d_{I-1} \\ & & & -d_I & d_I \end{bmatrix}, \tag{12}$$

where $d_i = (x_{i+1} - x_{i-1})^{-1}$ for $i = 2,3,\ldots,I-1$. The elements of the $\mathbf{d}$-matrix are chosen so that the weighted column sums should be identically zero. In addition to this condition, we have to impose the frequency boundary conditions on the elements of the first and last rows to account for the fact that the wings of the

line merge into continuum, which yields

$$d_1 = d_I = 0 \ . \tag{13}$$

The quantity $\mathbf{u}^{\pm}$ is the specific intensity vector.

To obtain a stable solution, we must decide on the step size τ_{crit} on the optical depth scale to obtain the reflection and transmission functions in a 'cell'. This is given by

$$\tau_{\text{crit}} = \min\{\tau_{k,k}, \tau_{k,k+1}, \tau_{k+1,k}\} \ , \tag{14}$$

where

$$\tau_{kk} < \left| \frac{2\mu_{kk} + \rho_c \Lambda^{+}_{kk} - d_{kk}\{\mu^2_{kk}\Delta V_{n+(1/2)} + \rho_c V_{n+(1/2)}(1-\mu^2_{kk})\}}{(\beta + \phi_{kk}) - \frac{1}{2}(1-\epsilon)(\phi\phi^T W)_{kk}} \right| \ , \tag{15}$$

$$\tau_{k,k+1} < \left| \frac{2\rho_c \Lambda^{+}_{k,k+1} - 2d_{k,k+1}\{\Delta V_{n+(1/2)}\mu^2_{k,k+1} + \rho_c V_{n+(1/2)}(1-\mu^2_{k,k+1})\}}{(1-\epsilon)(\phi\phi^T W)_{k,k+1}} \right| \tag{16}$$

and

$$\tau_{k+1,k} < \left| \frac{2\rho_c \Lambda^{+}_{k+1,k} + 2d_{k+1,k}\{\Delta V_{n+(1/2)}\mu^2_{k+1,k} + \rho_c V_{n+(1/2)}(1-\mu^2_{k+1,k})\}}{(1-\epsilon)(\phi\phi^T W)_{k+1,k}} \right| \ ; \tag{17}$$

where $k = j + (i-1)J$; i and j are frequency and angle indices, and I and J are the total number of frequency angle points. Moreover, the Λ's are the curvature matrices; and W's the quadrature weights for the angle-frequency integration points. It is interesting to note that the critical step-size is determined not only by ρ_c, μ's, Λ's, but also by the velocity of the medium and the elements of the **d** matrix.

3. Computational Procedure and Discussion of the results

Reflection and transmission operators are calculated by using the procedure mentioned in Paper I and the diffuse radiation field and the source functions are calculated by using the algorithm given in Peraiah and Grant (1973). In the case of star's rest frame (or observer's frame), we need a large number of frequency-angle points as the velocity between the rest point and the gas change continuously, which shifts the frequency points from inside to outside the line. Therefore, in the rest frame, one must take care that the frequency-angle mesh extends over the entire range $X \pm V_{\text{max}}$, where V_{max} is the maximum gas velocity, and the line transfer must be considered over this enlarged band width of the line. On the other hand, in a co-moving frame there are no relative velocities between the observer and the moving gas and one can employ the line profile function corresponding to a static medium. This means that we require only a small number of frequency-angle points. We have selected several sets of frequency grids for test purposes; 9, 13, 15, 19 frequency points in the line for

small optical depths of 100 for different gas velocities. The frequency-independent source functions corresponding to various frequency grids (S_9, S_{11}, S_{13}, S_{19}) for the same velocity law have been compared. Surprisingly, S_9 differs from S_{11} in the fourth decimal place, S_{11} differs from S_{13} in the sixth place and practically no difference from S_{13} onwards. However, when the maximum velocity reaches 80 or 90 mean thermal units, the error in S_9 increases and in no case exceeds 1% of the values at S_{19}. Therefore, one can use a frequency grid with 9 points for smaller velocities and a frequency grid with 11 or 13 points need be used for larger velocities.

We have selected trapezoidal points for frequency-grid and Gauss–Legendre points for angle integration. We have assumed complete re-distribution for the sake of simplicity and have employed Doppler profile (see Equation 3). Three types of media have been considered – e.g.,

$$\begin{aligned} &(1) \quad \epsilon = \beta = 0 \ , \\ &(2) \quad \epsilon = 10^{-3}, \beta = 0 \ , \\ &(3) \quad \epsilon = \beta = 10^{-3} \ . \end{aligned} \tag{18}$$

The first case corresponds to a purely scattering medium, the second case with line emission and the third case with both line and continuum emission. We must specify the boundary conditions on the specific intensities incident on either side of the medium and on the wing frequencies which appear in the derivative $\partial I/\partial x$. The boundary conditions are

$$\text{(i)} \quad \left\{ \begin{matrix} U^-_{N+1}(x_i, \tau = T, \mu_j) = 1 \\ U^+_1(x_i, \tau = 0, \mu_j) = 0 \end{matrix} \right\} \quad \text{for } \epsilon = \beta = 0 \ , \tag{19}$$

$$\text{(ii)} \quad \left\{ \begin{matrix} U^-_{N+1}(x_i, \tau = T, \mu_j) = 0 \\ U^+_1(x_i, \tau = 0, \mu_j) = 0 \end{matrix} \right\} \quad \epsilon, \beta > 0 \ , \tag{20}$$

where

$$\mathbf{U}^{\pm}_n = [\mathbf{U}^{\pm}_{1,n}, \mathbf{U}^{\pm}_{2,n}, \mathbf{U}^{\pm}_{3,n}, \ldots, \mathbf{U}^{\pm}_{i,n}, \ldots, \mathbf{U}^{\pm}_{I,n}]^T \ , \tag{21}$$

$$\mathbf{U}^{\pm}_{i,n} = 4\pi r_n^2 I(x_i, \pm\mu_j, r_n) \ ; \tag{22}$$

r_n being the outer radius of the shell n. Moreover,

(iii) in the continuum, we set $\partial I/\partial x = 0$, or

$$[\mathbf{d} \cdot \mathbf{U}^{\pm}_{n+(1/2)}]_{i=1 \text{ and } n} = 0 \ . \tag{23}$$

Equations (19), (20) and (23) will specify the boundary conditions of the problem. The total optical depth is taken to be 1500. We have employed velocity laws with positive and negative gradient, given by

$$V_n = V_A + n\Delta V_{n+(1/2)} \ , \tag{24}$$

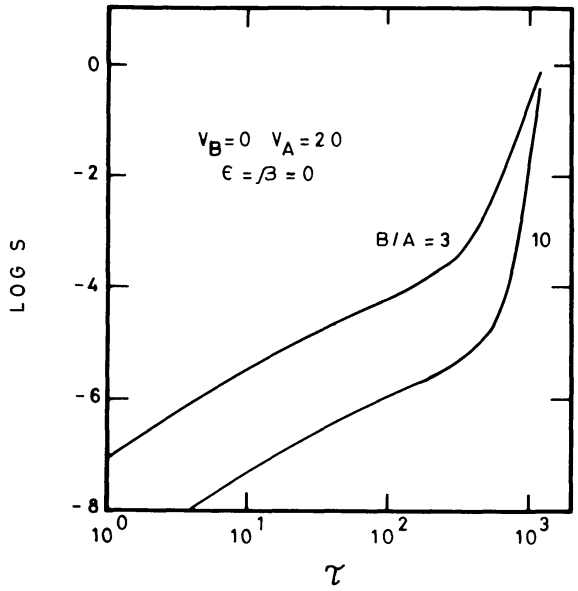

Fig. 1. Source functions are shown for a medium in which the gases are moving with negative velocity gradients.

where A and B are the inner and outer radii of the medium and

$$\Delta V_{n+(1/2)} = \frac{V_B - V_A}{N} \; ; \tag{25}$$

V_A and V_B being the velocities of the gas at A and B, respectively, in mean thermal units (mtu) and N is the total number of shells of equal geometrical thickness. The results are presented in Figures 1–12. In Figure 1, we have given the source function corresponding to a velocity law given in Equation (24) by

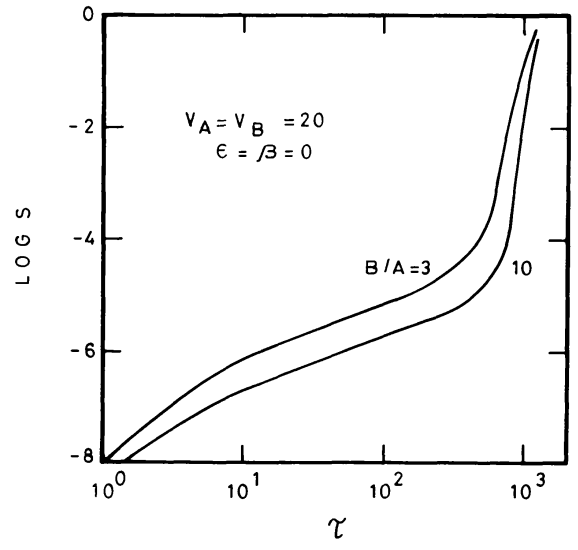

Fig. 2. Source functions are shown for a medium with constant gas velocities.

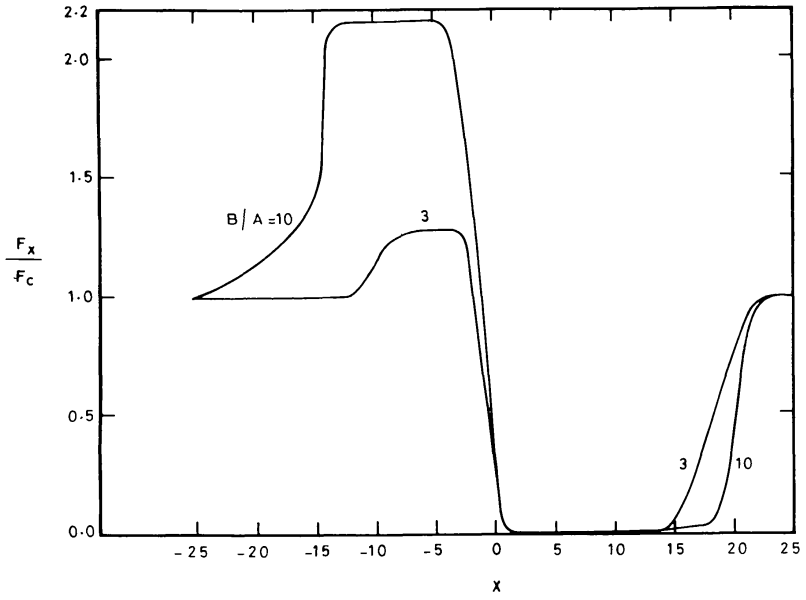

Fig. 3. Flux profiles corresponding to the source functions given in Figure 1.

setting $V_A = 20$ mtu, and $V_B = 0$, so that ΔV is negative. The maximum is at A, the inner radius, and the velocity changes roughly as $1/r$ in accordance with the equation of continuity. In Figure 2, we have given source functions corresponding to a constant velocity with 20 units of mean thermal velocity. In both cases we have set $\epsilon = \beta = 0$ and $B/A = 3$ and 10. We notice a large reduction in the source function by about 8 orders of magnitude from $r = A$ to $r = B$. The source

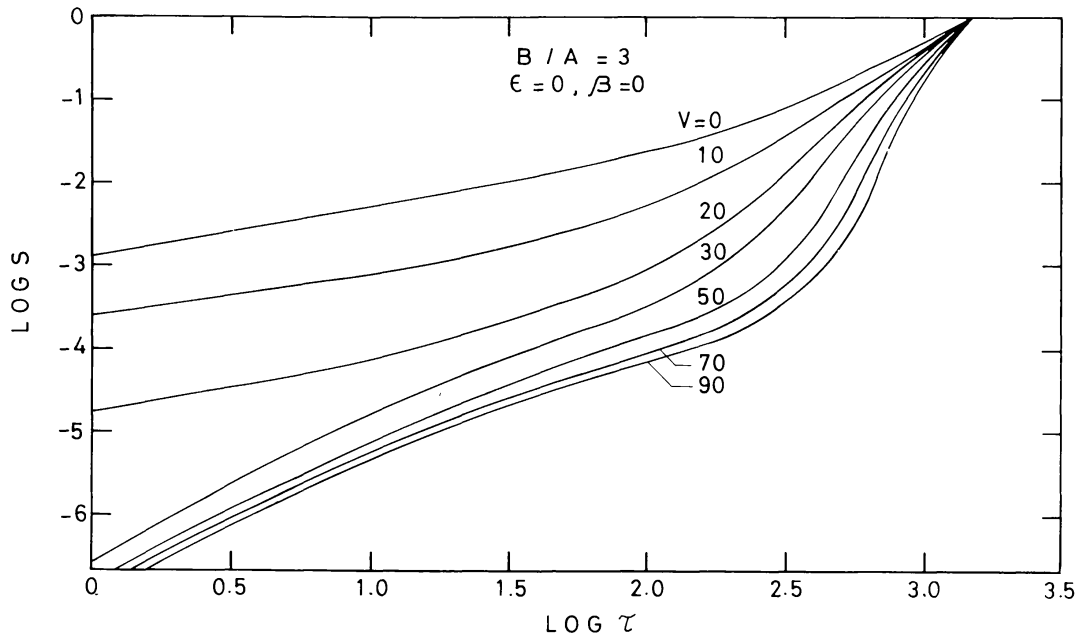

Fig. 4. Source functions for the medium with positive velocity gradients.

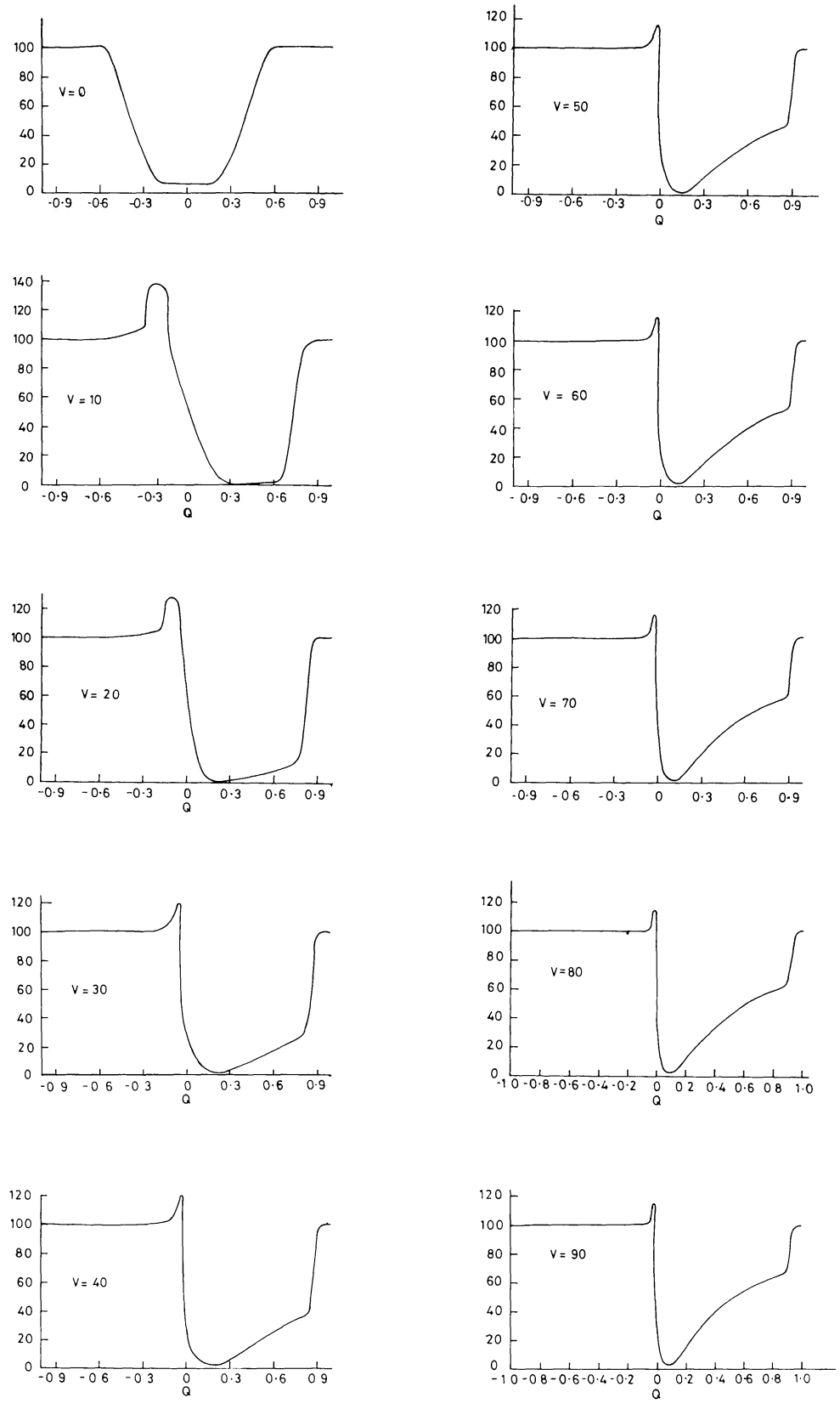

Fig. 5. Flux profiles corresponding to the source functions shown in Figure 4. $Q = X/X_{max}$.

function corresponding to $B/A = 3$ are generally larger than those corresponding to $B/A = 10$ by approximately an order of magnitude in the case of negative velocity gradients (Figure 1), whereas the differences in the source functions corresponding to $B/A = 3$ and 10 are smaller when we use a constant velocity, i.e., with zero velocity gradients. The source functions that we have presented are calculated in the co-moving frame. However, we need to calculate the line profiles at infinity so that these can be directly compared with observed profiles. The procedure is described in Paper II. The profiles corresponding to the source functions given in Figure 1 are given in Figure 3. The profiles corresponding to the source functions of Figure 2 are quite similar to those given in Figure 3 and, hence, are not presented here; while F_c is the flux in the continuum. We note that when $B/A = 3$, there is small emission on the red side of the centre of the line and deep absorption on the blue side. The emission and absorption are clearly separated. When B/A is set to 10, the emission further increases, although there is not much change in the absorption. This is because, when the atmosphere has much larger radius, the side lobes also increase. Consequently, more radiation is scattered and this is received by the observer. This is clearly a P Cygni-type profile.

In Figure 4, we have plotted the source functions corresponding to the velocity law with a positive velocity gradient so that the velocity increases constantly from $r = A$ to $r = B$. We always set $V_A = 0$ and changed the quantity V_B from 0 to 90 mtu in steps of 10 mtu. We have always set $\epsilon = \beta = 0$. The source functions are reduced considerably from $r = A$ to $r = B$. In the static case ($V_B = 0$) the reduction is by about 3 orders of magnitude whereas in the case of moving medium the reduction is towards the boundary $r = B$ is gradual. When the velocity reaches 90 mtu, the source function is reduced as much as 7 orders of magnitude. This is due to the fact that, as the matter moves fast, it will dilute the radiation field. The corresponding flux profiles are plotted in Figure 5 for $V_B = 0$ to 90. In a static medium ($V_B = 0$), we notice that a symmetric absorption line is formed. When a small amount of motion is introduced, a slight emission of about 35% above the continuum appears on the red side with deep absorption on the blue side. As the velocity increases further red emission is not as prominant as in the case of small velocities. The absorption part of the line becomes narrower.

In Figure 6, we have given the source functions for $\epsilon = 10^{-3}$, $\beta = 0$ and $V_B = 0$, 10, 30 and 60 and $B/A = 3$, 9. As there is no incident radiation at $\tau = \tau_{max}$, the source functions are smaller than those inside the medium. The corresponding flux profiles are given in Figures 7 and 8. In a static medium, we obtain symmetric profiles with emission and central absorption, whereas those profiles formed in a moving medium have nearly symmetric emission. For larger velocities, the flux profiles are almost symmetric and very similar to those found in some of the quasars (Baldwin, 1975; Baldwin and Netzer, 1978). Compare these profiles with those given in Figure 9 of Mihalas *et al.* (1975). The source

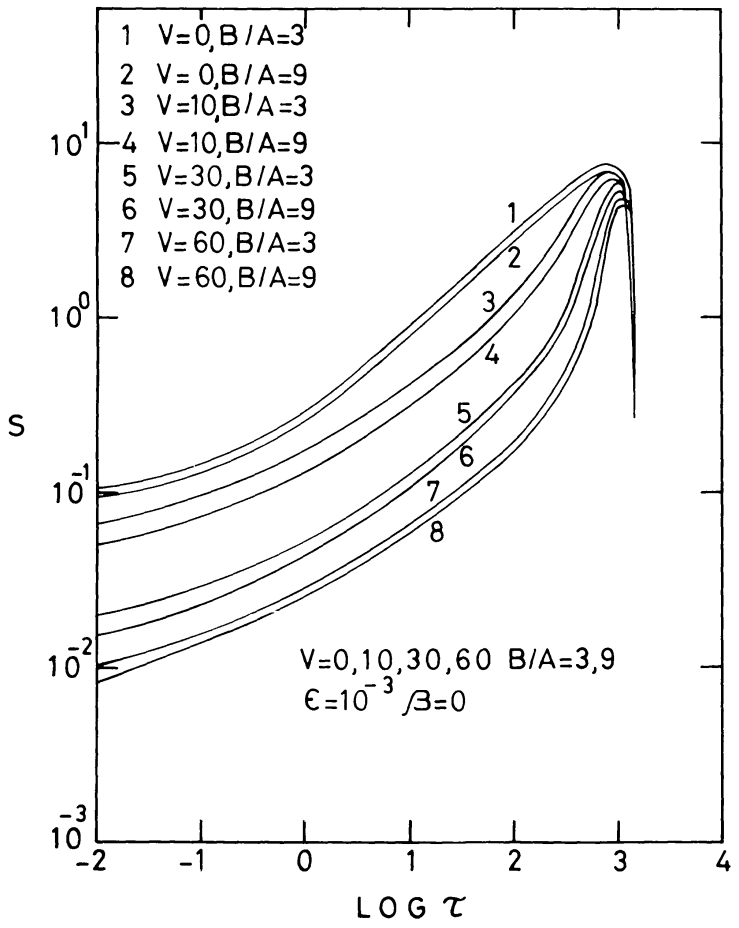

Fig. 6. Source functions for $\epsilon = 10^{-3}$, $\beta = 0$, and $B/A = 3$ and 9.

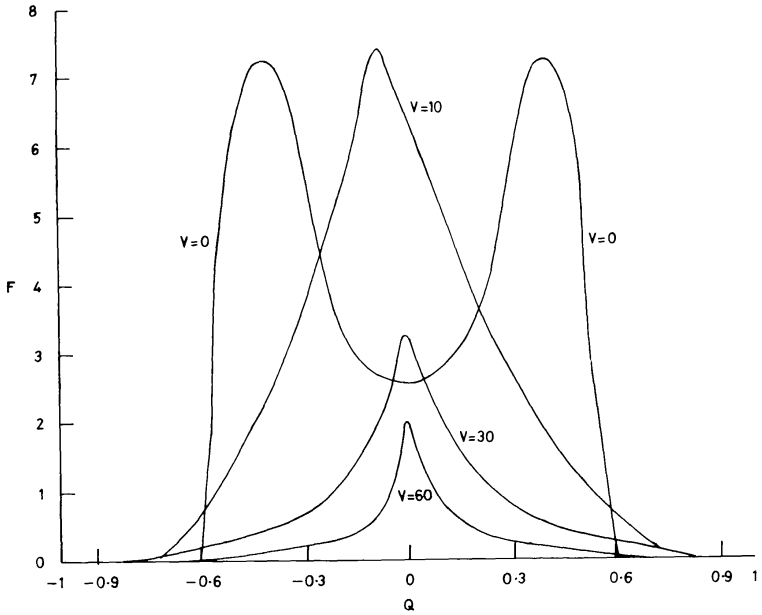

Fig. 7. Flux profiles corresponding to the source functions in Figure 6 with $B/A = 9$.

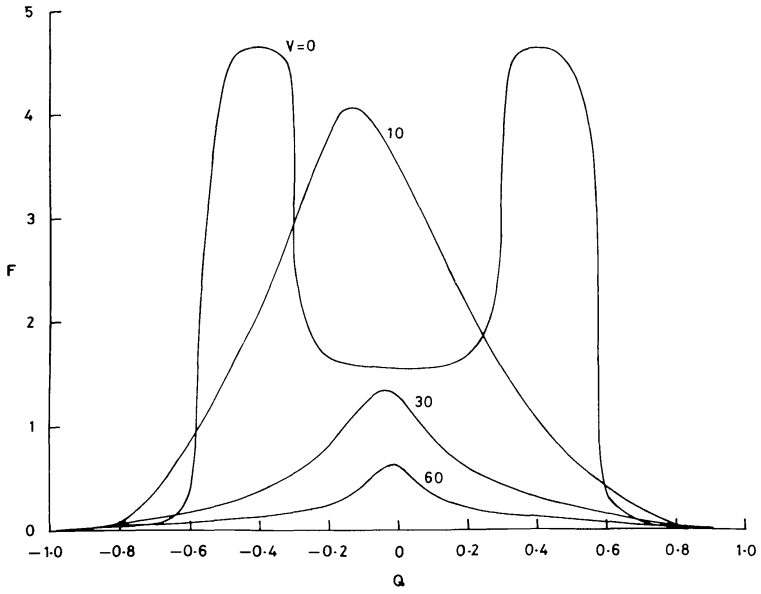

Fig. 8. Flux profiles corresponding to the source functions in Figure 6 with $B/A = 3$.

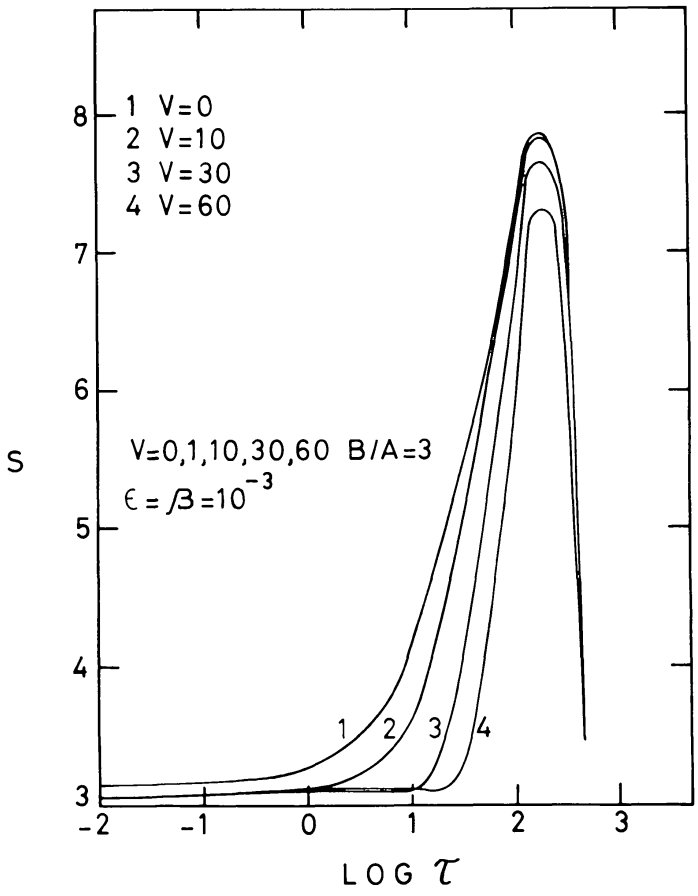

Fig. 9. Source functions with $\epsilon = \beta = 10^{-3}$ and $B/A = 3$.

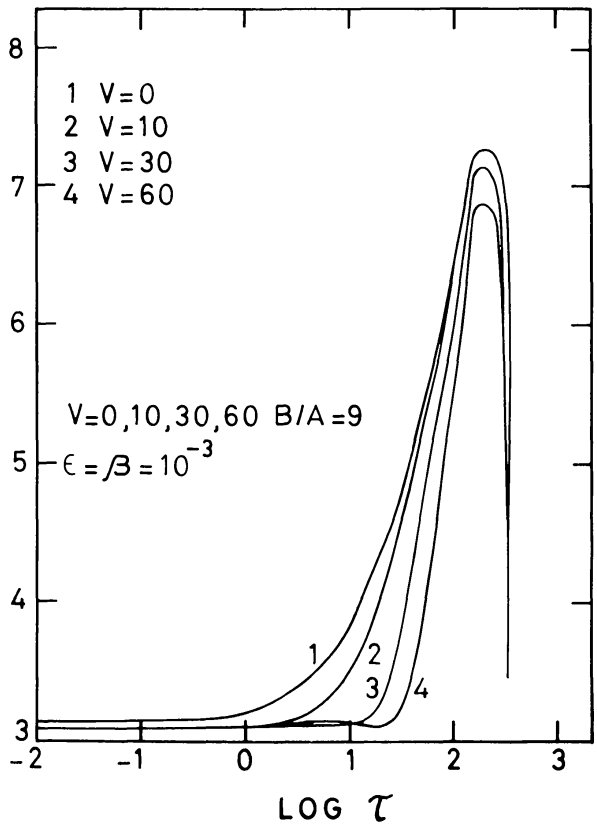

Fig. 10. Same as in Figure 9 with $B/A = 9$.

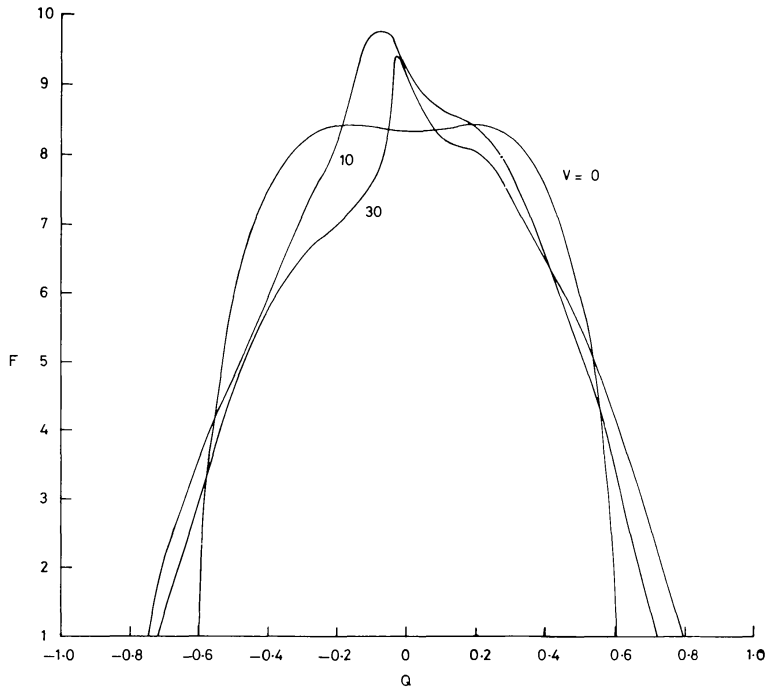

Fig. 11. Flux profiles corresponding to the source functions given in Figure 9.

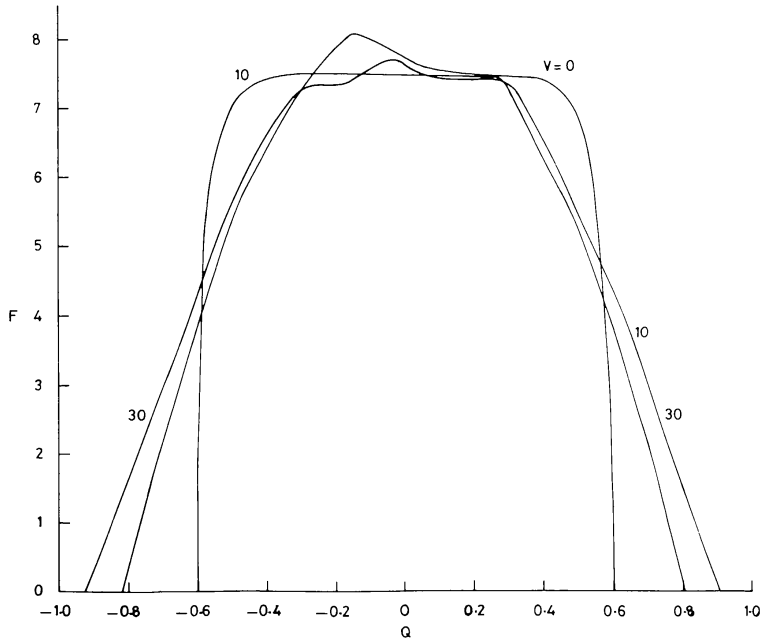

Fig. 12. Flux profiles corresponding to the source functions given in Figure 10.

functions corresponding to $\epsilon = \beta = 10^{-3}$ and $B/A = 3$ and 9 are given in Figures 9 and 10 and their corresponding flux profiles are given in Figures 11 and 12. Again these profiles are quite similar to those given in Figure 9 of Mihalas *et al.* (1975). These profiles are box-type emission lines and this increases with velocity and geometrical extension (see, for example, Bappu, 1973).

References

Baldwin, J. A.: 1975, *Astrophys. J.* **201**, 26.
Baldwin, J. A. and Netzer, H.: 1978, *Astrophys. J.* **226**, 1.
Bappu, M. K. V.: 1973, in M. K. V. Bappu and J. Sahade (eds.), 'Wolf-Rayet and High Temperature Stars', *IAU Symp.* **49**, 59.
Kunasz, P. B. and Hummer, D. G.: 1974, *Monthly Notices Roy. astron. Soc.* **125**, 21.
Mihalas, D., Kunasz, P.B. and Hummer, D.G.: 1975, *Astrophys. J.* **202**, 465.
Peraiah, A.: 1978, *Kodaikanal Obs. Bull.* **2**, 115.
Peraiah, A.: 1980a, *Acta Astron.* (in press).
Peraiah, A.: 1980b, *J. Astrophys. Astron.* **1**, 3.
Peraiah, A. and Grant, I. P.: 1973, *J. Inst. Math. Appl.* **12**, 75.
Simmonneau, E.; 1973, *Astron. Astrophys.* **29**, 357.